LES Study of Combustion Dynamics and NO_x Emissions in a Full-Scale Hydrogen-Air Rotating Detonation Engine

Pinaki Pal
Transportation and Power Systems Division, Argonne National Laboratory
Lemont, IL, USA

Peter A. Strakey, Donald H. Ferguson
National Energy Technology Laboratory
Morgantown, WV, USA

1 Introduction

Detonation-based pressure gain combustion (PGC) concepts, offering much higher thermodynamic efficiency and compactness relative to deflagrative combustion, have been extensively researched over the last two decades for a wide variety of propulsion and power generation applications [1]. Among PGC technologies, rotating detonation engines (RDEs) have garnered the most attention [2, 3]. Moreover, hydrogen-fueled RDEs are deemed to be particularly attractive for decarbonization of the stationary power generation sector owing to their immense potential as a carbon-neutral high-efficiency alternative to traditional land-based gas turbine combustors.

In practical rotating detonation combustor (RDC) configurations, the fuel and oxidizer are continuously injected (through separate slots or discrete ports) at one end of an annular combustion chamber, while one or more self-sustained detonation waves propagate azimuthally within the chamber near the injection plane and process the fuel-oxidizer mixture into products. This results in steady work output at high frequencies. In addition, non-premixed fuel-oxidizer injection prevents detonation flashback into the feed plenums. RDCs exhibit complex flow-fields with moving detonation/shock waves and highly unsteady fluctuations in temperature and pressure. The performance of RDCs is intricately related to a number of factors, such as fuel/oxidizer composition, operating conditions (global equivalence ratio, inlet mass flow rates and temperatures, back pressure, etc.), injection schemes, detonation channel geometry, and coupling with other components of the engine such as upstream feed plenums and downstream turbomachinery [2, 3]. As such, system-level integration aspects need to be taken into account when considering practical deployment of RDCs. For example, the interaction between the detonation waves and discrete fuel/oxidizer injection schemes leads to incomplete and inhomogeneous fuel-oxidizer mixing, unsteady injector flow behavior, premature (parasitic) deflagration, and post-detonation (commensal) combustion, that have significant influence on detonation strength/stability and achievable pressure gain [4-8]. On the other hand, when integrating an RDC with turbomachinery, the impact of oblique shock waves poses major challenges. The RDC exhaust flow is unsteady, transonic, spatially non-uniform, and swirling in nature [9, 10], which can negatively impact turbine efficiency and durability [11-12]. Recent studies [13-16] have investigated the impact of coupling RDCs with converging/diverging transition elements and nozzle guide vanes (NGV) to appropriately condition the inlet flow to the turbine. In addition, a few experimental [17] and numerical [18-21] studies have been

Correspondence to: pal@anl.gov

carried out to investigate the emissions of nitrogen oxides (NO_x) from RDCs, which is an important consideration for stationary power generation applications.

In the above context, this work presents a high-fidelity large-eddy simulation (LES) study of a full-scale water-cooled hydrogen-air RDC integrated with a downstream exhaust diffuser. The computational fluid dynamics (CFD) model is validated against experimental data pertaining to number of waves, wave speed, nitric oxide (NO) emissions exiting the RDE, and axial pressures at the RDC outer wall. The numerical results are further analyzed to characterize the RDC combustion and NO_x emissions behavior.

2 Experimental Setup and Operating Conditions

Experiments were performed in a water-cooled RDC [22] at the Applied Thermal Sciences Laboratory within U.S. Department of Energy's National Energy Technology Laboratory in Morgantown, West Virginia. The RDC includes a ducted exhaust and a high-temperature, back-pressure control valve that provides the ability to control the pre-combustion back-pressure independent of any restriction at the RDC exit plane. The back-pressure control valve also serves to simulate the presence of a turbine downstream of the RDC. Both the internal and external structures of the assembly are water-cooled to support long-duration testing. Tests performed for this study were limited to 20-30 second duration to conserve fuel (hydrogen) while permitting the combustor and immediate exhaust components to reach a state of thermal equilibrium. A cross-sectional view of the RDC along with a profile view of the axial pintle-style fuel injector are shown in Fig. 1. The RDC has a 7.53 cm long detonation channel with an outer diameter, D_{outer}, of 14.88 cm and gap width of 1.02 cm. The axial injector consists of a minimal injection area ($A_{3.1}$) of 16.11 cm^2 resulting in a ratio of channel area to injector area ($A_{3.2}/A_{3.1}$) of 2.7. After the detonation channel, there is a 1.44 cm long area restriction, that reduces the gap size to 0.76 cm resulting in an exit area to channel area ratio of ($A_8/A_{3.2}$) of 0.76. Immediately downstream of the exit restriction is an exhaust diffuser designed to efficiently expand the detonation products prior to entering a hypothetical turbine.

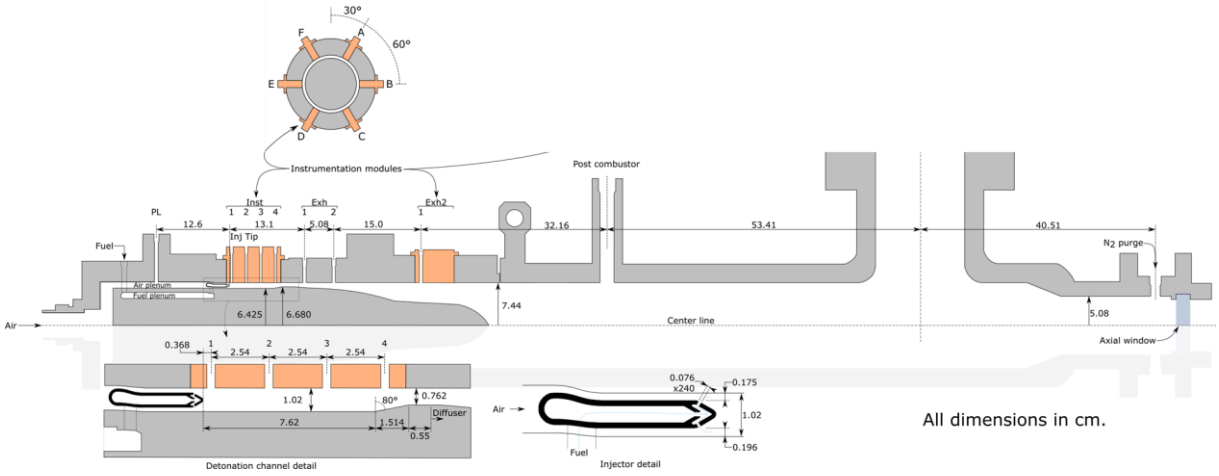

Figure 1: Schematic of the NETL RDC-diffuser configuration [22].

Six instrumentation modules are located along the RDC wall at 60° circumferential intervals, with each port containing four access points, two of them being visible in the cross-sectional view provided in Fig. 1. The modules are designated A-F going clockwise from top dead center when looking downstream along the combustor axis. Each port is given a number designation (1, 2, 3, 4) with the first port (1) located ~3.7 mm from the downstream tip of the pintle injector and subsequent ports are positioned 25.4 mm further downstream. A second ring of six instrumentation modules is located just downstream of the RDC exit nozzle restriction, and a third ring is located near the diffuser exit. A series of pressure

transducers are located in ports E1 – E4 in a capillary tube averaged pressure (CTAP) configuration in order to provide a measure of static pressure along the length of the combustor. Viscous effect of the capillary tubes eliminates the unsteady (periodic) pulses in pressure associated with the propagating detonation waves. In this work, two operating conditions (with hydrogen as fuel and air as oxidizer) were simulated, which are listed in Table 1.

Table 1: RDC operating conditions for simulated cases.

Case	Fuel/Air mass flow rate (kg/s)	Global equivalence ratio	Fuel/Air inlet temperature (K)	Backpressure (kPa)
1	0.01362/0.5218	0.894	330/432	131
2	0.01191/0.5621	0.725	331/431	133

3 Numerical Modeling Approach

A commercial CFD solver, CONVERGE [23], was employed for performing LES of the full-scale RDC-diffuser configuration. A predetonator tube was added to the combustor to initiate detonation in the annular chamber. A base mesh size of 1.5 mm was used with three levels of fixed region embedding (cell size of 0.01875 mm) at the pintle injector orifices and two levels of fixed region embedding (cell size of 0.375 mm) within the fuel injection ports and fuel inlet tubes. Two levels of fixed boundary embedding (cell size of 0.375 mm) was specified near the walls of the intake plenums, combustor, and diffuser. Fixed region embedding with two levels was prescribed within the predetonator tube. In addition, four levels of spherical embedding (cell size of 0.09375 mm) were imposed at the far end of the predetonator tube to resolve the spark ignition kernel. Lastly, one level of adaptive mesh refinement (AMR) was employed in the intake plenums and diffuser, and three levels of AMR (minimum grid size of 0.1875 mm) were used in the combustor. Each simulation corresponded to ~32 million grid points. It must be noted that in 3D detonations with non-premixed injection and finite mixing, the detonation process is highly non-ideal, leading to broad (thickened) detonation zones and induction lengths (approx. an order of magnitude larger than that of an ideal detonation case). The grid resolution used here results in at least 10 cells across the broadened induction length, and is therefore appropriate for the LES study.

Full set of governing transport equations for compressible reacting flow corresponding to mass, momentum, total internal energy, and chemical species mass fractions were solved in the LES framework. A second-order-accurate spatial discretization scheme (with step flux limiter) was used for the governing equations with a fully-implicit first-order-accurate time integration scheme. A single-species diffusion model was used with turbulent Prandtl number of 0.7 and turbulent Schmidt number of 0.98. The mixture specific heat capacity was computed as mass fraction-weighted average of the specific heat capacities of individual species. The dynamic structure model [24] was used for subgrid turbulence closure. The law-of-the-wall boundary condition for velocity was applied to all the walls. On the other hand, an isothermal boundary condition of 300 K was imposed at the walls and the model proposed by Angelberger [25] was employed to account for wall heat transfer. An ideal gas equation of state was used as the constitutive relation. In addition, a variable time-stepping algorithm was employed in the current study with a minimum time step of 1 ns. The time step during simulation was calculated automatically by the solver during each computational cycle based on the maximum allowed Courant-Friedrichs-Levy (CFL) numbers of 0.5, 2.0 and 0.5, corresponding to convection, diffusion and speed of sound, respectively. A detailed hydrogen-air kinetic mechanism (9 species, 21 reactions) [26] coupled with NO_x chemistry (10 species, 41 reactions) [27] was used with a finite-rate chemistry model [28-30], which excludes subgrid turbulence-chemistry interaction effects [31-32]. Constant mass flow rates from experiments were imposed at the fuel and air inlets, while a transonic boundary condition was prescribed at the outlet.

Each LES was initialized with both the RDC and predetonator tube (with the interface between them kept closed) at a uniform temperature of 300 K and pressure corresponding to the prescribed back pressure, with the combustor filled with air and the predetonator tube filled with stoichiometric hydrogen-oxygen mixture. Then, a non-reacting flow simulation was performed until steady state was reached. Thereafter, this steady flow solution was used as initial condition for the reacting flow simulation. The predetonator tube was spark ignited at one end, leading to reaction front propagation and deflagration-to-detonation-transition (DDT) within the tube. The interface between the RDC channel and the predetonator tube was then opened for a short duration, thereby allowing the detonation wave to enter the annulus and initiate detonation in the chamber. After the initiation of RDC ignition, the interface was closed for the remainder of the simulation. The flow was then allowed to evolve in the RDC. Quasi-steady state was considered to have been achieved after 7-8 detonation wave cycles with fixed wave mode were observed without significant changes in the wave speed.

4 Results and Discussion

CFD simulations for both the conditions result in two-wave mode, which is consistent with experiments. For Case 1, the predicted and measured wave speeds are 1703 m/s and 1599 m/s, respectively. On the other hand, LES and experiment yield wave speeds of 1663 m/s and 1605 m/s, respectively, for Case 2. Although wave speeds are over-predicted in simulations, discrepancy of ~100 m/s is considered to be a reasonable agreement with experiments. As for the time-average of the mass-weighted average NO concentration exiting the combustor, the LES predict 97 ppmv and 77 ppmv for Cases 1 and 2, respectively, on a wet basis. The corresponding experimental measurements are 23.15 ppmv and 18 ppmv. Therefore, the simulations predict the NO_{exit} trend correctly, with overprediction of ~4.2x. The NO discrepancy between simulations and experiments can be potentially attributed to the overprediction of detonation wave speed (and thereby strength) and preclusion of turbulence-chemistry interaction effects in the combustion modeling approach [19]. Lastly, the axial static pressures at E1/E2/E3/E4 port locations predicted by LES are found to be in good agreement with the corresponding CTAP measurements for both Case 1 (predicted: 2.25/1.94/1.77/1.73 bar; measured: 2.04/1.9/1.68/1.67 bar) and Case 2 (predicted: 2.35/2.24/1.92/1.79 bar; measured: 2.15/2.01/1.85/1.77 bar).

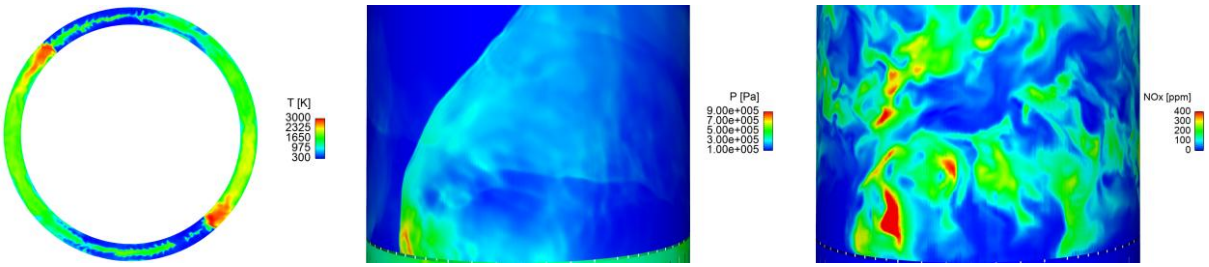

Figure 2: Instantaneous snapshots of static temperature on a horizontal cut-plane passing through the detonation waves and fill region (left), static pressure at RDC mid-channel (center), and NO_x concentration at RDC mid-channel (right) for Case 1.

The instantaneous snapshot of static temperature for Case 1 shown in Fig. 2 clearly depicts the two primary detonation waves. Significant deflagrative burning in the fill region can be observed ahead of the detonation waves, known as parasitic combustion. On the other hand, it is evident from the instantaneous static pressure and NO_x concentration snapshots that NO_x is predominantly formed behind the detonation waves, where static temperatures are relatively higher. It is also found that NO concentrations are three orders-of-magnitude greater than nitrogen dioxide (NO_2) concentrations.

5 Conclusions

High-fidelity reacting LES of a full-scale hydrogen-air RDC-diffuser configuration were performed under multiple operating conditions, employing finite-rate chemistry with a detailed H_2-air-NO_x kinetic mechanism and leveraging AMR for computational efficiency. The numerical results were validated against available experimental data pertaining to wave mode/speed, axial pressures at the RDC outer wall, and exit NO emissions. The analysis of LES results shows parasitic combustion in the fill region, NO_x formation primarily behind the detonation waves, and NO as the dominant NO_x species.

6 Acknowledgements

The submitted manuscript has been created by UChicago Argonne, LLC, Operator of Argonne National Laboratory (Argonne). Argonne, a U.S. Department of Energy Office of Science laboratory, is operated under Contract No. DEAC02-06CH11357. The U.S. Government retains for itself, and others acting on its behalf, a paid-up nonexclusive, irrevocable worldwide license in said article to reproduce, prepare derivative works, distribute copies to the public, and perform publicly and display publicly, by or on behalf of the Government. This research was funded by the DOE Office of Fossil Energy and Carbon Management (FECM)'s Advanced Turbines Program with Mathew F. Adams as the program monitor. The authors would like to acknowledge the compute allocations on Improv and Bebop clusters provided by the Laboratory Computing Resource Center (LCRC) at Argonne National Laboratory. In addition, the authors thank Convergent Science, Inc., for providing CONVERGE CFD software licenses.

References

[1] P. Wolanski, Detonative propulsion, *Proc. Combust. Inst.*, 34 (2013) 125-158.

[2] V. Raman, S. Prakash, M. Gamba, Non-idealities in rotating detonation engines, *Annual Rev. Fluid Mechanics*, 55 (2023) 639-674.

[3] V. Anand, E. Gutmark, Rotating detonation combustors and their similarities to rocket instabilities, *Prog. Energy Combust. Sci.*, 73 (2019) 182-234.

[4] F. Chacon, M. Gamba, Study of parasitic combustion in an optically accessible continuous wave rotating detonation engine, *AIAA Paper* 2019-0473 (2019).

[5] S. Prakash, V. Raman, C. Lietz, W.A. Hargus, S.A. Schumaker, High fidelity simulations of a methane-oxygen rotating detonation rocket engine, *AIAA Paper* 2020-0688 (2020).

[6] P. Pal, S. Demir, S. Som, Numerical modeling of combustion dynamics in a full-scale rotating detonation rocket engine using large eddy simulations, *J. Energy Res. Technol.*, 145 (2022) 021702.

[7] P. Pal, C. Xu, G. Kumar, S.A. Drennan, B.A. Rankin, S. Som, Large-eddy simulation and chemical explosive mode analysis of non-ideal combustion in a non-premixed rotating detonation engine, *AIAA Paper* 2020-2161 (2020).

[8] P. Pal, C. Xu, G. Kumar, S. Drennan, B.A. Rankin, S. Som, Large-eddy simulations and mode analysis of ethylene/air combustion in a non-premixed rotating detonation engine, *AIAA Paper* 2020-3876 (2020).

[9] D.L. Depperschmidt, J.R. Tobias, R.S. Miller, M. Uddi, A.K. Agrawal, J.B. Stout, Time-resolved PIV diagnostics to measure flow-field exiting methane-fueled rotating detonation combustor, *AIAA Paper* 2019-1514 (2019).

[10] V. Athmanathan, K. A. Rahman, D. K. Lauriola, J. Braun, G. Paniagua, M. N. Slipchenko, S. Roy, T. R. Meyer, Femtosecond/picosecond rotational coherent anti-Stokes Raman scattering thermometry in the exhaust of a rotating detonation combustor, *Combust. Flame*, 231 (2021) 111504.

[11] D.E. Paxson, A. Naples, Numerical and analytical assessment of a coupled rotating detonation engine and turbine experiment, *AIAA Paper* 2017-1746 (2017).

[12] Z. Liu, J. Braun, G. Paniagua, Performance of axial turbines exposed to large fluctuations, *AIAA Paper* 2017-4817 (2017).

[13] J. Braun, B.H. Saracoglu, G. Paniagua, Unsteady performance of rotating detonation engines with different exhaust nozzles, *J. Propuls. Power*, 33 (2017) 121-130.

[14] S. Talukdar, D. Langner, A. Gupta, A.K. Agrawal, Performance characteristics of a rotating detonation combustor exiting into a pressurized plenum to simulate gas turbine inlet, *J. Energy Res. Technol.* (2023).

[15] P. Pal, J. Braun, K. Karimli, V. Athmanathan, G. Paniagua, T.R. Meyer, Large-eddy simulations of a hydrogen-air non-premixed rotating detonation combustor coupled with a downstream nozzle, *AIAA Paper* 2023-4271 (2023).

[16] P. Pal, J. Braun, Y. Wang, V. Athmanathan, G. Paniagua, T.R. Meyer, Large-eddy simulation study of flow and combustion dynamics in a full-scale hydrogen-air rotating detonation combustor-stator integrated system, *J. Eng. Gas Turbines Power*, 147 (2024) 031002.

[17] D.H. Ferguson, B. O'Meara, A. Roy, K. Johnson, Experimental measurements of NO_x emissions in a rotating detonation engine, *AIAA Paper* 2020-0204 (2020).

[18] D.A. Schwer, K. Kailasanath, Characterizing NO_x emissions for air-breathing rotating detonation engines, *AIAA Paper* 2016-4779 (2016).

[19] P.A. Strakey, D.H. Ferguson, Experimental measurements and CFD predictions of NO_x emissions from a water-cooled rotating detonation engine, *ASME Turbo Expo Paper* GT2023-100851 (2023).

[20] C. Van Beck, V. Raman, Influence of detonation waves on NO_x emissions in rotating detonation engines using Lagrangian particle tracking, *AIAA Paper* 2024-1423 (2024).

[21] C. Van Beck, V. Raman, NO_x formation processes in rotating detonation engines, *Front. Aerosp. Eng.*, 3 (2024) 1335906.

[22] J. Weber, C. Bedick, C. Albunio, T. Sidwell, D. Ferguson, Choked flow in a converging/diverging rotating detonation engine exit, *AIAA Paper* 2023-1500 (2023).

[23] P.K. Senecal, K.J. Richards, E. Pomraning, T. Yang, M.Z. Dai, R.M. McDavid, M.A. Patterson, S. Hou, T. Shethaji, A new parallel cut-cell CFD code for rapid grid generation applied to in-cylinder diesel engine simulations, *SAE Technical Paper* 2007-01-0159 (2007).

[24] S.G. Chumakov, C.J. Rutland, Dynamic structure subgrid-scale models for large eddy simulation, *Int. J. Numer. Methods Fluids*, 47 (2005) 911-923.

[25] C. Angelberger, T. Poinsot, B. Delhay, Improving near-wall combustion and wall heat transfer modeling in SI engine computations, *SAE Technical Paper* 972881 (1997).

[26] M. O'Conaire, H. Curran, J.M. Simmie, W.J. Pitz, C.K. Westbrook, A comprehensive modeling study of hydrogen oxidation, *Int. J. Chem. Kinetics*, 36 (2004) 603-622.

[27] Chemical-Kinetic Mechanisms for Combustion Applications, San Diego Mechanism web page, Mechanical and Aerospace Engineering (Combustion Research), University of California at San Diego (http://combustion.ucsd.edu).

[28] P. Pal, S. Demir, P. Kundu, S. Som, Large-eddy simulations of methane-oxygen combustion in a rotating detonation rocket engine, *AIAA Paper* 2021-3642 (2021).

[29] P. Pal, G. Kumar, S.A. Drennan, B.A. Rankin, S. Som, Multidimensional numerical modeling of combustion dynamics in a non-premixed rotating detonation engine with adaptive mesh refinement, *J. Energy Res. Technol.* 143 (2021) 112308.

[30] P. Pal, G. Kumar, S.A. Drennan, B.A. Rankin, S. Som, Numerical modeling of supersonic combustion in a non-premixed rotating detonation engine, *11th US National Combustion Meeting* (2019).

[31] P. Pal, S. Keum, H.G. Im, Assessment of flamelet versus multi-zone combustion modeling approaches for stratified-charge compression ignition engines, *Int. J. Engine Res.*, 17 (2016) 280–290.

[32] S. Keum, P. Pal, H.G. Im, A. Babajimopoulos, D.N. Assanis, Effects of fuel injection parameters on the performance of homogeneous charge compression ignition at low-load conditions, *Int. J. Engine Res.*, 17 (2016) 413–420.